

Bioinspired Ultrastrong Solid Electrolytes with Fast Proton Conduction along 2D Channels

Guangwei He, Mingzhao Xu, Jing Zhao, Shengtao Jiang, Shaofei Wang, Zhen Li, Xueyi He, Tong Huang, Moyuan Cao, Hong Wu, Michael D. Guiver,* and Zhongyi Jiang*

Solid electrolytes have attracted much attention due to their great prospects in a number of energy- and environment-related applications including fuel cells. Fast ion transport and superior mechanical properties of solid electrolytes are both of critical significance for these devices to operate with high efficiency and long-term stability. To address a common tradeoff relationship between ionic conductivity and mechanical properties, electrolyte membranes with proton-conducting 2D channels and nacre-inspired architecture are reported. An unprecedented combination of high proton conductivity (326 mS cm^{-1} at $80 \text{ }^\circ\text{C}$) and superior mechanical properties (tensile strength of 250 MPa) are achieved due to the integration of exceptionally continuous 2D channels and nacre-inspired brick-and-mortar architecture into one materials system. Moreover, the membrane exhibits higher power density than Nafion 212 membrane, but with a comparative weight of only ≈ 0.1 , indicating potential savings in system weight and cost. Considering the extraordinary properties and independent tunability of ion conduction and mechanical properties, this bioinspired approach may pave the way for the design of next-generation high-performance solid electrolytes with nacre-like architecture.

Solid electrolytes that conduct ions (particularly protons) have attracted much attention due to their prospects in a number of energy- and environment-related applications including

Dr. G. He, M. Xu, J. Zhao, S. Wang, Z. Li, X. He, T. Huang,
Prof. M. Cao, Prof. H. Wu, Prof. Z. Jiang
Key Laboratory for Green Chemical Technology of Ministry of Education
School of Chemical Engineering and Technology
Tianjin University
Tianjin 300072, China
E-mail: zhyjiang@tju.edu.cn

Dr. G. He, M. Xu, J. Zhao, S. Wang, Z. Li, X. He, T. Huang, Prof. H. Wu,
Prof. M. D. Guiver, Prof. Z. Jiang
Collaborative Innovation Center of Chemical Science
and Engineering (Tianjin)
Tianjin 300072, China
E-mail: michael.guiver@outlook.com

S. Jiang
School of Civil & Environmental Engineering
Georgia Institute of Technology
Atlanta, GA 30332, USA

Prof. M. D. Guiver
State Key Laboratory of Engines
School of Mechanical Engineering
Tianjin University
Tianjin 300072, China

DOI: 10.1002/adma.201605898

fuel cells, lithium-ion batteries, flow batteries, and electro dialysis.^[1] Fast ion transport and superior mechanical properties for solid electrolytes are both of critical significance for these devices to operate with high efficiency and long-term stability.^[2] However, a tradeoff relationship commonly exists between ionic conductivity and mechanical properties.^[1,3] A frequently exploited approach to address this issue leverages the hydrophilic-hydrophobic bicontinuous nanophase morphologies of block copolymers to independently control the ion conductivity and mechanical properties.^[4,5] Nevertheless, some limitations of this approach encompass (i) insufficient ion conductivity at low humidity due to the lack of long-range order in the conducting channels, and (ii) relatively low mechanical strength due to the lack of hierarchically designed nonionic phases. Moreover, the resulting complex nanophase structures confound

the fundamental understanding of the ion-conducting behavior. Another important approach is the fabrication of composite solid electrolytes reinforced by strong porous substrates such as porous polytetrafluoroethylene, porous polyimide, glass-fiber paper, and nonwoven fabrics.^[6] While this has certain merits, the durability of the solid electrolytes could be degraded due to weak interactions and surface energy differences between the substrate and impregnated electrolyte. Furthermore, the ion conductivity could be compromised by the nonconductive substrates. Thus, a novel approach that integrates both superior ion conduction and mechanical properties within one material is imperative.

2D materials of atomic thickness such as graphene oxide (GO) and montmorillonite (MMT) have emerged as ideal molecular building blocks to develop intricately structured advanced membranes.^[7] The 2D building blocks can be easily assembled into lamellar microstructures showing ordered channels that percolate throughout the membrane as well as being highly uniform and tunable in width. Consequently, membranes incorporating 2D channels have demonstrated extraordinarily rapid mass transport.^[8] However, studies of 2D channel solid electrolyte membranes are still in their infancy,^[9] and fast ion conduction channels that can compete effectively in performance with those in block copolymer membranes have not yet been created. Nanochannels containing high concentrations of

sulfonic acid groups can enable superior proton conductivity in that the strongly acidic groups impart a highly dissociated ion concentration as well as well-connected water network structures. Such a favorable chemical microenvironment facilitates proton conduction.^[10] Thus, it is conjectured that high proton conductivity could be obtained if highly sulfonated electrolytes are incorporated into the interlayer space of the 2D channels, because both the physical and chemical microenvironments are optimized for proton transport. However, 2D membranes have been challenged with inferior mechanical properties due to inadequate interlayer adhesion.^[11]

Coincidentally, 2D materials are utilized as building blocks in nature to construct armor having exceptional mechanical properties, exceeding the majority of artificial materials for self-protection, which offers ingenious inspiration to address the aforementioned issue.^[12] Nacre possesses highly sophisticated structures with well-ordered brick-and-mortar architecture composed of about 95 vol% 2D calcium carbonate and 5 vol% biopolymers. The high-level ordering of the inorganic 2D nanosheets coupled with robust organic–inorganic interfaces confers highly efficient load transfer between the organic moiety and inorganic moiety, leading to exceptional mechanical properties.^[13,14] Thus, it is envisaged that superior mechanical properties could be achieved if nacre-like nanostructures are incorporated into the 2D solid electrolytes.

Herein, we report for the first time the fabrication of nacre-inspired proton-conducting solid electrolytes through controlled assembly of the 2D materials (GO and MMT nanosheets) and highly sulfonated hydrophilic polymer (sulfonated polyvinyl alcohol, SPVA) along with rational manipulation of the inorganic–organic interfacial interactions. Two types of 2D materials are utilized to implement a synergistic toughening effect. An unprecedented combination of high proton conductivity (326 mS cm⁻¹ at 80 °C) and superior mechanical properties (tensile strength of 250 MPa) are achieved due to the integration of 2D channels and nacre-inspired brick-and-mortar architecture into one materials system. Our study indicates that enabling the independent tunability of ion-conduction and mechanical properties is an effective approach to designing next-generation high-performance solid electrolytes for established and emerging energy and environmental applications.

SPVA was synthesized by the reaction of polyvinyl alcohol with benzaldehyde-2,4-disulfonic acid disodium salt

(BADSA).^[14,15] The chemical structure of SPVA is confirmed by ¹H nuclear magnetic resonance (¹H NMR) spectrum (Figure S1, Supporting Information), which shows signals between 7.7 and 8.2 ppm (d₁–d₃) corresponding to the protons of benzene in BADSA. The content of sulfonic acid groups or ion exchange capacity (IEC) in SPVA is 4.21 mmol g⁻¹, which is calculated based on the signal area ratios of the protons d₁–d₃ and *a*. The content of hydroxy groups in SPVA is 5.05 mmol g⁻¹, which is calculated based on the signal area ratios of protons *c* and *a*. GO was synthesized by the modified Hummers method^[16] and the structures are verified by atomic force microscopy (AFM), wide angle X-ray diffraction (XRD), and X-ray photoelectron spectroscopy (XPS), as shown in Figure S2 (Supporting Information). The thickness and in-plane size of individual GO nanosheets are around 1 nm and 1–2 μm, respectively, as observed by AFM. The sharp peak (2θ = 10.79) in the XRD pattern indicates that the interlayer spacing of GO nanosheets is 0.82 nm. The XPS pattern shows typical peaks of GO at binding energies of 282 and 530 eV, corresponding to C 1s and O 1s, respectively.^[17] The high oxygen content (38.9 wt%) indicates a high degree of oxidation of GO due to the presence of abundant hydroxy, epoxy, and carboxyl groups.^[18] The structures of MMT are determined by transmission electron microscopy (TEM), XRD, and XPS, as shown in Figure S3 (Supporting Information). The TEM images show that the in-plane size of MMT nanosheets was 0.1–0.3 μm. The sharp peak (2θ = 6.2°) in the XRD pattern indicates that the interlayer spacing of MMT nanosheets is 1.4 nm.

The GO/MMT/SPVA ternary composite membranes were fabricated by a vacuum-assisted self-assembly method, as illustrated by Figure 1a.^[19] It is noteworthy that the underlying reason of utilizing a ternary composite is that nacre-inspired ternary composites show higher mechanical properties than other binary composites due to the effective synergistic toughening effect from incorporating two kinds of 2D nanomaterials.^[20] The weight ratio of GO to MMT for all the composite membranes was maintained at 9:1, which is selected based on previous literature.^[21] For the GO/MMT/SPVA-*X* (*X* = 30, 40, 50, 60) membranes, *X* corresponds to the weight ratio of SPVA to [GO + MMT + SPVA] in the filtration suspension. The weight of glutaraldehyde (GA: cross-linker) was 1.6 times of that of SPVA. The actual mass fractions of SPVA were estimated by thermogravimetric analysis (TGA), as shown in Figure S4 and

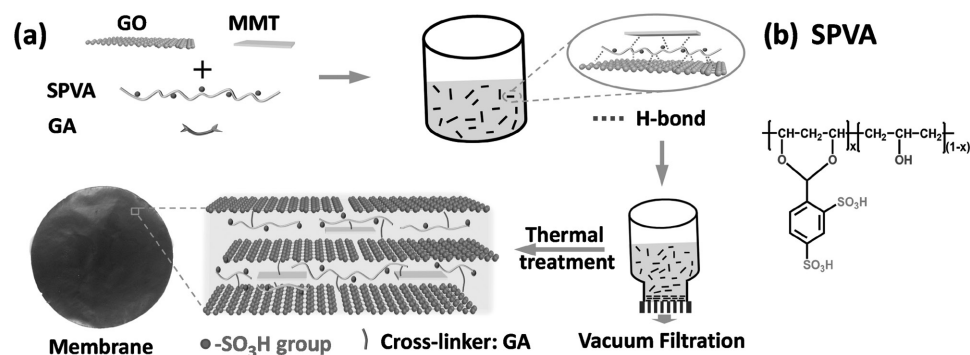


Figure 1. a) Schematic illustration of preparing GO/MMT/SPVA composite membranes and digital picture of the membrane. b) Chemical structure of SPVA.

Table S1 (Supporting Information). Both the 2D nanoscale building blocks (GO and MMT) and SPVA have a large number of polar groups (hydroxy, epoxy, carboxy groups) to ensure the hydrogen-bonding driven assembly during the preliminary physical blending process, resulting in sandwich-structured nanosheets.^[19,22] By using vacuum filtration, the ternary composite membrane was formed.

The cross-sectional morphologies of the GO/MMT/SPVA composite membranes were observed by scanning electron microscopy (SEM) (Figure 2a–d). The membranes reveal well-ordered laminar microstructures, which are similar to the brick-and-mortar structure of nacre and many other nacre-inspired materials.^[23,24] A comparison between Figure 2 and Figure S5 (Supporting Information) highlights the striking similarities between the GO/MMT/SPVA membranes and natural nacre.^[23,25] The 2D nanosheets in the membranes are broadly orientated horizontally. With an increasing content of SPVA, the sharp profile of the 2D nanosheets becomes less distinct due to the increased amount of polymer enveloping the nanosheets. The distribution of Si (a characteristic element in MMT) and S (a characteristic element in SPVA) in the GO/MMT/SPVA-30 membrane, probed by energy-dispersive X-ray spectroscopy (EDX) mapping and shown in Figure S7 (Supporting Information), indicates a homogeneous distribution of MMT and SPVA throughout the membrane. XRD spectroscopy was used to further confirm the “brick-and-mortar” microstructure of the GO/MMT/SPVA membranes, as shown in Figure S8 (Supporting Information). With an increasing content of SPVA, the *d*-spacing of GO in the membranes increases from 0.96 to 1.34 nm, implying the ordered arrangement of GO nanosheets and increased content of polymers in the GO interlayers. The peaks corresponding to MMT are not observed due to the low content of MMT in the composites.

To evaluate the mechanical properties of the nacre-inspired membranes, we measured the stress–strain curves, as shown in Figure 3 and Table S2 (Supporting Information). The

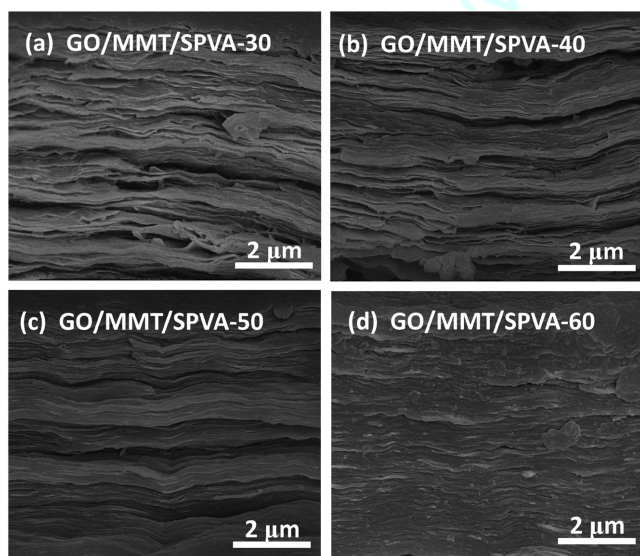


Figure 2. a–d) SEM cross-sectional images of the GO/MMT/SPVA membranes.

GO/MMT/SPVA membranes exhibit exceptionally high tensile strength and elastic modulus, surpassing those of all reported proton-conducting electrolyte membranes (PEMs) (Figure 4d; Table S6, Supporting Information). The GO/MMT/SPVA-30 membrane shows the highest mechanical properties with a tensile strength of 288 MPa and elastic modulus of 18.63 GPa, in contrast to some state-of-the-art poly(aryl ether) block copolymer electrolytes exhibiting a tensile strength of about 48.5 MPa and an elastic modulus of about 1.7 GPa.^[26] Such superior mechanical properties can be attributed to the nacre-like brick-and-mortar architecture of GO/MMT/SPVA membranes.^[27] Nacre possesses two distinct structural features: (i) the horizontal orientation of 2D inorganic materials; (ii) the strong interfacial interactions between 2D materials and polymers.^[13,28] The superior load-transfer efficiency between the flexible polymers and stiff inorganic materials endows nacre with high mechanical properties. According to the above SEM and XRD characterizations, the GO/MMT/SPVA membranes exhibited nacre-like architecture with horizontally orientated GO and MMT as “bricks,” which are glued together by SPVA and GA molecules as “mortar.” SPVA contains a high density of hydroxy and ether groups, which readily form numerous hydrogen bonds with oxygen-containing groups on GO nanosheets and siloxane units on MMT nanosheets. Moreover, SPVA forms C–O–Al covalent bonds with MMT nanosheets, as confirmed by Fourier transform infrared (FTIR) (Figure S10, Supporting Information); the introduction of GA in the filtration solution strengthens the covalent bonding between 2D materials and polymers (Figure S8, Supporting Information).^[14] GA is an efficient cross-linking agent that forms covalent acetal linkages between hydroxy groups from SPVA, GO, and MMT nanosheets.^[19] The synergy between hydrogen bonds and covalent bonds affords the GO/MMT/SPVA membranes robust interfacial adhesion, thus promoting load transfer efficiency.^[29] It is noteworthy that the presence of sulfonic acid groups is detrimental to interfacial adhesion in the interlayers, as indicated by the result in Figure S11b (Supporting Information), although this is somewhat counteracted by cross-linking with GA. In the absence of polymer being utilized in membrane formation, insufficient hydrogen bonds between the 2D inorganic nanosheets results in lower strength and toughness of the GO and GO/MMT membranes compared with natural nacre (tensile strength of 80–135 MPa and toughness of 1.8 MJ m⁻³).^[25] Through the fine-tuning of the organic/inorganic interfacial interactions via the incorporation of SPVA and cross-linker, the mechanical properties of GO/MMT/SPVA membranes are remarkably improved. The GO/MMT/SPVA-50 membrane shows tensile strength of 250.2 MPa and toughness of 2.7 MJ m⁻³, which are about 85% and 50% higher than those of natural nacre counterpart. The mechanical properties are also higher than many other nacre-inspired materials, as shown in Table S3 (Supporting Information). With increasing SPVA in 2D nanosheet galleries, the tensile strength tends to decrease from 287.7 to 180.7 MPa because the increased polymers densely wrap the GO and MMT nanosheets and reduce the interlayer adhesion.^[30]

To determine the optimal dosage of GA, GO/MMT/SPVA-50-I (low cross-linking degree) and GO/MMT/SPVA-50-II (high cross-linking degree) membranes are fabricated as a comparison

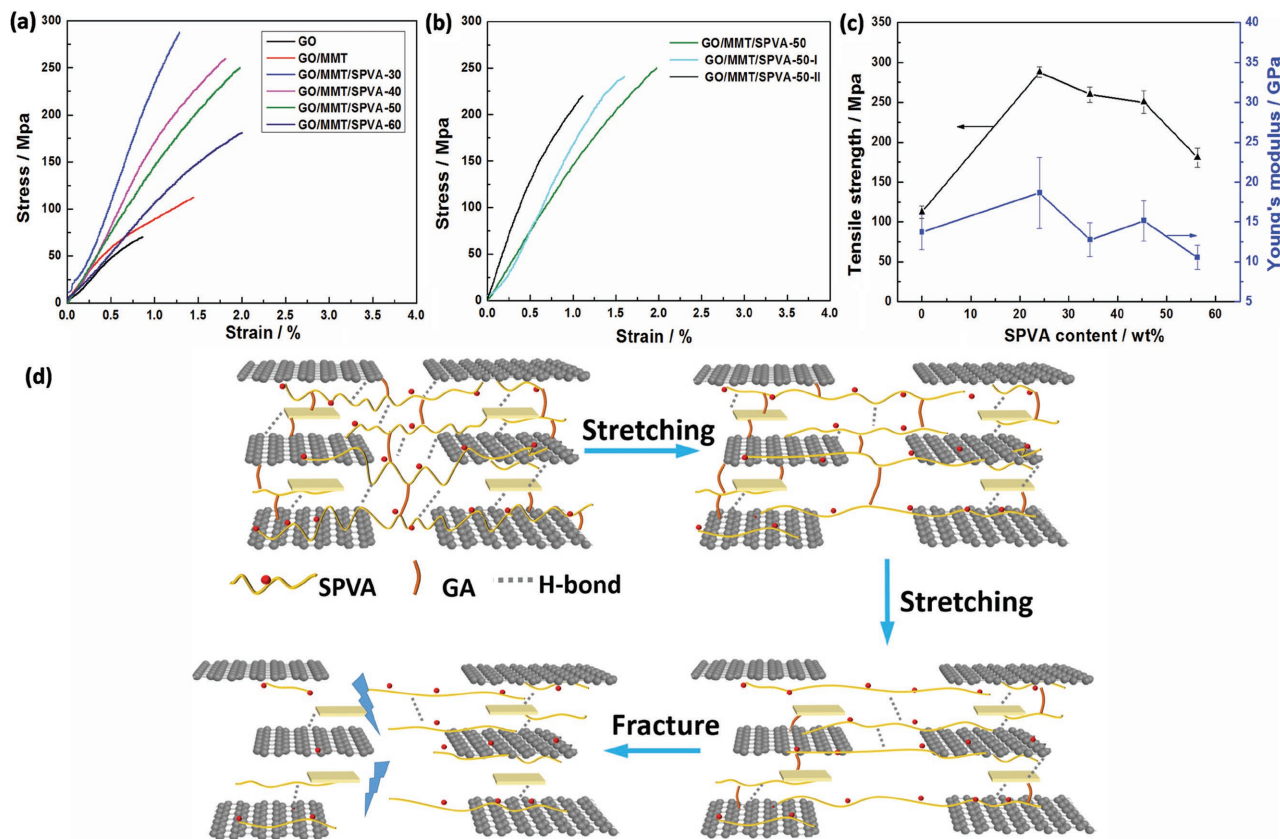


Figure 3. a) Tensile stress–strain curves of GO/MMT/SPVA membranes. b) Comparison of tensile stress–strain curves of GO/MMT/SPVA membranes with different degrees of cross-linking. c) The tensile strength and Young's modulus of GO/MMT/SPVA membranes with different SPVA contents. d) Proposed synergistic mechanism of nacre-inspired GO/MMT/SPVA membrane.

and the mechanical properties are shown in Figure 3b. The result indicates that moderate cross-linking degree is beneficial to the enhancement of mechanical properties. Owing to higher dosage of GA, the GO/MMT/SPVA-50 membrane possesses stronger interfacial interactions, higher tensile strength, and elastic modulus in comparison with GO/MMT/SPVA-50-I membrane. With further increasing the GA cross-linking agent (double that of GO/MMT/SPVA-50-I), the GO/MMT/SPVA-50-II membrane shows decreased tensile strength and toughness because of excessive cross-linking; the membrane is brittle and ruptures at a relatively low elongation.^[31]

To elucidate the synergistic strengthening effect of the ternary composite GO/MMT/SPVA membrane, a fracture model is proposed (Figure 3d). With initial stretching, the nanosheets slide over each other. The weaker hydrogen bonds between the 2D nanosheets and SPVA are first broken, followed by stretching of the coiled SPVA long chains, leading to dissipation of energy. Subsequently, the friction between GO nanosheets and MMT nanosheets brings about the movement of MMT along GO. With the gradual increase of loading, the covalent bonds at the interfaces are broken and more energy is absorbed, leading to pull-out of the nanosheets and destruction of the membranes, as shown in the fracture morphology of Figure S9 (Supporting Information).

The mechanical bendability test results of the GO/MMT/SPVA membranes are shown in Figure S12 (Supporting

Information). All the membrane samples maintain their dimensional stability after 100 bending cycles, indicating that the GO/MMT/SPVA membranes have a strong resistance to fracturing or cracking when subjected to bending stress. As shown in Figure S13 (Supporting Information), the membranes maintained their mechanical properties after compression at a pressure of 1 MPa, indicating that the membranes have a high resistance to compression. Dynamic mechanical analysis (DMA) of GO/MMT/SPVA-50 membrane (Figure S14, Supporting Information) indicates that the storage modulus of the membrane is close to its Young's modulus, and the storage modulus increases with temperature.

The chemical stability of PEMs is crucial for their practical application in fuel cells.^[32] Table S5 (Supporting Information) shows the results of the accelerated oxidative stability of the GO/MMT/PVA membranes in Fenton's reagent, indicating the membranes' resistance to free radical attack. The weight losses of the membranes were all above 90 wt% after 1 h exposure, and the membranes did not dissolve even after 50 h exposure. The GO/MMT/PVA membranes exhibit better oxidative stability in comparison to many aromatic sulfonated PEMs treated under the same conditions.^[33] This excellent stability arises primarily from the narrow transport channels and cross-linked chemical structures in the GO/MMT/PVA membranes, and the good chemical stability of graphene.^[34]

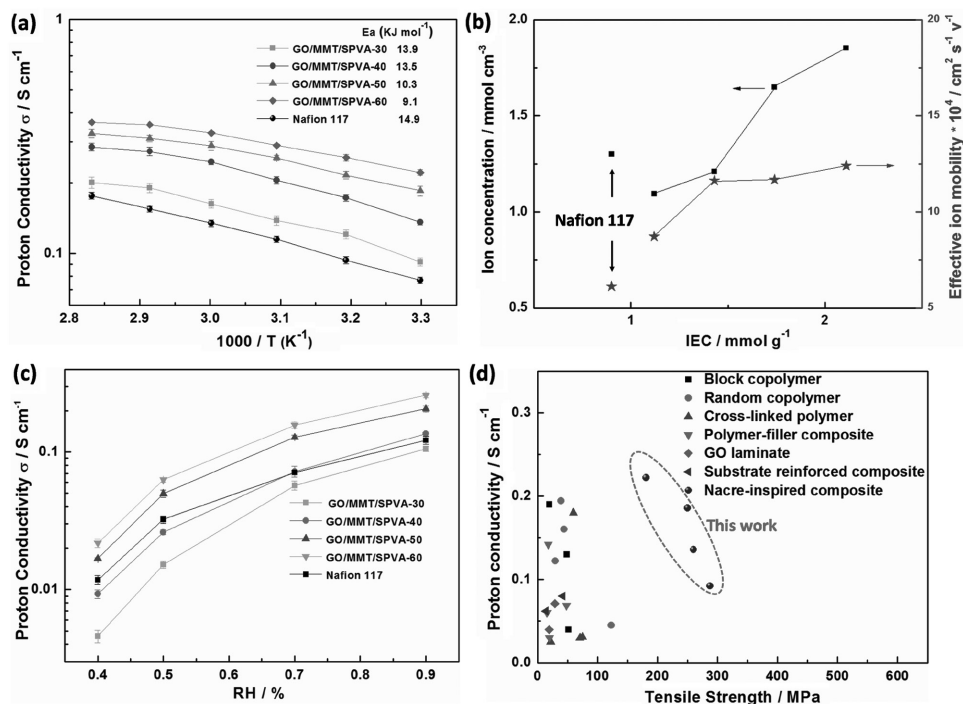


Figure 4. a) Proton conductivity of GO/MMT/SPVA and Nafion 117 membranes as a function of time at 100%RH. b) Ion concentration and effective ion mobility of GO/MMT/SPVA and Nafion 117 membranes as a function of IEC. c) Humidity dependence of the GO/MMT/SPVA and Nafion 117 membranes at 80 °C. d) Comparison of proton conductivity and tensile strength of the present nacre-inspired membranes and other typical PEMs. The data in (d) are presented in Table S6 (Supporting Information).

To evaluate the proton transport properties of the 2D channels, we investigate the proton conductivity of the GO/MMT/SPVA membranes in detail (Figure 4; Table S5, Supporting Information). The proton conductivities of the membranes positively correlate with the IEC. With increasing IEC from 1.12 to 2.11 mmol g⁻¹, the proton conductivity at 30 °C increases from 92 to 222 mS cm⁻¹, which is 2.9 times higher than that of Nafion 117, and 17% higher than that of a state-of-the-art block copolymer.^[5] The underlying reasons are summarized as follows: (i) with increasing IEC, the ion concentration of membranes increases as shown in Figure 4b; (ii) with increasing IEC, the size of 2D nanochannels increases as shown by XRD. This improved physical microenvironment of ion nanochannels reduces the resistance of proton transport and thus facilitates the ion mobility, which is in good accordance with the result shown in Figure 4b. Such a simultaneous increase of ion concentration and ion mobility leads to the enhancement of proton conductivity. Figure 4a shows that the proton conductivity of the membranes increases with temperature, which arises from the thermally activated characteristic of proton transport. The activation energy (E_a) is calculated according to the Arrhenius formula, and the result is shown in the insertion of Figure 4a. With increasing IEC, the membranes display decreased E_a , indicating the reduction of energy barrier for proton transport.^[35] This result is in good accordance with the enhancement of proton mobility shown in Figure 4b.

The GO/MMT/SPVA-60 membrane exhibits the highest proton conductivity, 364 mS cm⁻¹ at 80 °C and 100%RH, which is among the highest conductivity ever reported for a

moderately low IEC value.^[36] The conductivity is 257% higher than a state-of-the-art GO-based laminar membrane,^[37] and comparable to some state-of-the-art highly sulfonated block copolymers^[4,5,38] such as cross-linked sulfonated multiblock copoly(ether sulfone) with an IEC of 2.99 mmol g⁻¹ showing a conductivity of ≈ 340 mS cm⁻¹ at 80 °C and 95%RH.^[39] The high conductivity of GO/MMT/SPVA-60 is attributed to the following aspects: (i) the proton-conduction nanochannels of the GO/MMT/SPVA-60 membrane have a favorable chemical microenvironment. The hydration number λ (H₂O/fixed ionic charge) of the membrane is 14, as shown in Table S4 (Supporting Information). According to the literature, this degree of hydration is especially advantageous for proton transport; that is to say, the water content is sufficiently high to dissociate $-SO_3H$ groups and sustain high hydronium ion concentration (by avoiding the dilution effect).^[1] Moreover, the proton-conduction nanochannels are composed principally of highly sulfonated PVA (IEC 4.21 mmol g⁻¹), and thus have a high local ion concentration.^[38,40] Furthermore, the sulfonic acid group is identified as one of the most effective proton-conduction functionalities due to its strong acidity and superior hydration capability;^[40] (ii) the proton-conduction nanochannels of the GO/MMT/SPVA-60 membrane possess appropriate physical microenvironments. The membrane has predominately continuous 2D nanochannels percolating throughout the layered materials, affording the membrane low proton conduction resistance and energy barrier.^[41] The synergistic optimization of both the chemical and physical microenvironments endows the membrane with exceptionally high proton conductivity.

Compared with Nafion 117, the GO/MMT/SPVA-30 membrane shows higher proton conductivity at 100%RH, despite the ion concentration being considerably lower (see Figure 4a,b). This behavior further substantiates the excellent microenvironments of the nanochannels within the GO/MMT/SPVA membranes.

Figure 4c shows the humidity dependence of proton conductivity at 80 °C for the GO/MMT/SPVA and Nafion 117 membranes. The GO/MMT/SPVA-X (X is in the range of 40–60) membranes exhibit much higher or similar proton conductivity compared with Nafion 117 at a 40% to 90%RH range. In particular, the GO/MMT/SPVA-60 membrane has a proton conductivity of 62.6 mS cm⁻¹ at 50%RH, which is the highest value for all GO-based laminar membranes,^[42] and even comparable to the pioneering sulfonated nanoporous silica membrane (≈70 mS cm⁻¹ at 50%RH).^[43] The high conductivity can also be attributed to the appropriate microenvironments of the 2D nanochannels. The high density of –SO₃H groups favors the formation of well-connected water structures, even at low water content.^[44] In the case of the GO/MMT/SPVA-30 membrane, the proton conductivity shows a significant decrease with reducing RH, which may be the result from the collapse of relatively narrow nanochannels with water evaporation.

By integrating 2D channels into a nacre-inspired structure, the GO/MMT/SPVA membranes achieve an unprecedented combination of high proton conductivity and mechanical properties, as show in Figure 4d and Table S6 (Supporting Information). Remarkably, the GO/MMT/SPVA membranes exhibit up to 17 times higher tensile strength and up to nearly three orders of magnitude higher Young's modulus in comparison with those of typical solid electrolytes. In typical PEM structures, the proton conductivity is sustained by the hydrophilic phase while the mechanical properties are sustained by the hydrophobic phase.^[1] We provide a systematic comparison and discussion of different approaches to tuning the ion-conducting and mechanical properties of solid electrolytes in the Supporting Information (below Table S6). By contrast, the proton conductivity in GO/MMT/SPVA membranes is sustained by the 2D channels percolated throughout the electrolyte, while the mechanical properties are sustained by the nacre-like hierarchical brick-and-mortar architecture. This intriguing design is expected to open a new avenue to fabricate ion-conducting solid electrolytes with both high conductivities and superior mechanical properties.

To demonstrate the application potential of the ultrathin nacre-inspired membrane in a fuel cell, a polarization curve in a single cell membrane electrode assembly (MEA, operated at 40 °C and 60%RH) is measured, as shown in Figure S15 (Supporting Information). The maximum power density of the freestanding GO/MMT/SPVA-50 membrane (7 μm) is 159 mW cm⁻², which is 54% higher than that of Nafion 117 (183 μm) and 20% higher than that of Nafion 212 (50.8 μm). To the best of our knowledge, this is the thinnest free-standing PEM utilized for fuel cell application. The realization of our ultrathin PEM is enabled by the creation of nacre-like architecture. It is also noteworthy that the weight of the tested GO/MMT/SPVA-50 membrane per unit area is ≈0.03 that of Nafion 117 and ≈0.1 that of Nafion 212, indicating that the cost of fuel cell could be substantially reduced by applying the ultrathin GO/MMT/SPVA-50 membrane. Since the thermal

stability of the membranes is limited by the inferior stability of GO, future studies will be focused on improving the long-term stability of the membranes at elevated temperatures.

In summary, GO/MMT/SPVA ternary composite membranes with fast proton-conducting 2D channels and nacre-inspired architecture are fabricated for the first time. The GO/MMT/SPVA-60 membrane shows proton conductivity of 364 mS cm⁻¹ at 80 °C, 100%RH, which is among the highest ion conductivities ever reported. Such a high conductivity is attributed to the high density of sulfonic acid groups and exceptional continuity of the 2D channels. Owing to the brick-and-mortar architecture and strong interfacial interactions, the GO/MMT/SPVA membrane exhibits the highest tensile strength and Young's modulus ever reported for PEMs. Moreover, the GO/MMT/SPVA-50 membrane exhibits higher power density than Nafion 212 membrane, but with weight ≈0.1 that of Nafion 212 membrane, indicating potential savings in system weight and cost. Considering the extraordinary properties and independent tunability of ion conduction and mechanical properties of PEMs, this bioinspired approach may pave the way to the design of next-generation high-performance solid electrolytes with brick-and-mortar nacre-like architecture.

Experimental Section

Preparation of GO and MMT Dispersion: GO dispersion was synthesized according to the modified Hummers method,^[16] which was described in detail in a previous study.^[17] Briefly, a mixture of 98 wt% H₂SO₄ (115 mL), 5 g of graphite powder, and 5 g of NaNO₃ was mechanically stirred at 0 °C in a 1 L three-necked, round-bottomed flask, followed by the slow addition of 15 g of KMnO₄ (caution: fast addition of KMnO₄ may ignite the mixture!). The mixture was stirred at 0 °C for 2 h, and then stirred at 35 °C for 30 min. After 230 mL of water was added slowly during a period of 30 min, stirring was maintained at 98 °C for 3 h. Subsequently, the mixture was poured into water, followed by the addition of 30 mL of H₂O₂. Finally, the mixture was washed with 1 L of HCl (1 M), and then with excess water until the pH reached 7. The GO aqueous dispersion was obtained by dispersing the above product in water using ultrasonic treatment for 1 h. The GO aqueous dispersion was centrifuged at 3000 rpm for 40 min to remove the sedimentary GO (unexfoliated GO or large GO sheets). MMT aqueous dispersion was obtained by mechanically stirring 3 g of MMT in 500 mL of water for one week, followed by centrifuging at 3000 rpm for 20 min to remove the sedimentary MMT (unexfoliated MMT or large MMT sheets).^[21]

Preparation of SPVA: SPVA was synthesized by an acid-catalyzed reaction between hydroxy and aldehyde groups.^[15] 1 g of PVA was dissolved in 20 mL of water by stirring the solution at 95 °C for 4 h. Subsequently, 10 mmol of BADSA and 1 mL HCl (1 M) were added into the solution. The above mixture was stirred at 50 °C for 96 h, followed by repeatedly washing with ethanol, and then drying.

Preparation of GO/MMT/SPVA, GO/MMT, GO, and MMT Membranes: The preparation of GO/MMT/SPVA-X is described in detail as follows: (1) A specific amount of GO was dispersed in water (the concentration of GO was 2 mg mL⁻¹) under ultrasonic treatment for 1 h. Subsequently, a specific amount of MMT solution with a concentration of 2.7 mg mL⁻¹ was added into the above solution, followed by ultrasonic treatment for 1 h to obtain an aqueous dispersion of GO/MMT mixture; (2) A specific amount of SPVA aqueous solution (5 wt%) was added into the above GO/MMT mixture, followed by stirring for 2 h to obtain aqueous dispersion of GO/MMT/SPVA mixture; (3) A specific amount of GA was added into the above GO/MMT/SPVA mixture, followed by stirring for 2 min; and (4) The above homogeneous mixture was assembled into GO/MMT/SPVA-X membrane by vacuum filtration

of the mixture through a porous poly(ether sulfone) (PES) membrane having an average pore diameter of 220 nm), followed by thermal treatment at 60 °C for 12 h. The GO/MMT/SPVA-X membrane was peeled off from the PES membrane for the subsequent characterization and measurement. For the GO/MMT/SPVA-X (X = 30, 40, 50, 60) membranes, the X refers to the mass percentage of SPVA in the filtration mixture of GO, MMT, and SPVA. The weight ratio of GO to MMT is 9:1, and the weight ratio of GA to SPVA is 160%. Through adding different amounts of GA in the mixture, GO/MMT/SPVA membranes were fabricated with various degrees of cross-linking. The mass ratios of GA to SPVA in GO/MMT/SPVA-50-I (low cross-linking degree), GO/MMT/SPVA-50 (moderate cross-linking degree), and GO/MMT/SPVA-50-II (high cross-linking degree) are 100%, 160%, and 200%, respectively. The comparative GO/MMT, GO, and MMT membranes were prepared by a similar approach. In the GO/MMT membrane, the weight ratio of GO to MMT was also 9:1 for direct comparison. Most of the membranes used for characterization and measurement are 7 μm thick, as determined by a digital micrometer caliper (Mitutoyo). Only for the characterization of membrane cross-sectional morphology by SEM, 10 μm thick membrane was used for better visualization because the 7 μm thick membrane was easily curved.

Characterization: Cross-section morphology of the composite membrane was observed by field emission SEM (Nanosem 430) after being sputtered with a thin layer of platinum. The element distribution in the composite membrane was detected by EDX equipped SEM. FTIR spectra of the membrane samples were obtained with a Bruker Vertex 70 FTIR spectrometer equipped with a horizontal attenuated transmission accessory. The characterization of ¹H NMR spectrum was described in previous literature.^[45] The crystalline properties of GO/MMT/SPVA, GO/MMT, and GO membrane samples were measured by wide-angle XRD using a D/MAX-2500 X-ray diffractometer (Cu Kα). The thermal properties of the GO/MMT/SPVA and GO/MMT membrane samples were measured by TGA (NETZSCH-TG209 F3) at a heating rate of 10 °C min⁻¹ under an N₂ atmosphere. The surface morphology of GO was observed by AFM (CSPM 5000). The surface morphology of MMT was observed by TEM (Tecnai G2 20 S-TWIN).

Proton conductivity of the membrane samples was tested by two-point probe alternating current (AC) impedance spectroscopy using an electrode system connected with a frequency response analyzer (Compactstat, IVIUM Tech.). Proton conductivity under 100%RH was tested in a temperature-controlled water-bath chamber. Proton conductivity under low RH (40%–90%) was tested in a temperature and humidity controlled chamber. Proton conductivity (σ , S cm⁻¹) was calculated according to the equation: $\sigma = l/AR$, where R is the resistance, A is the cross-sectional area of the sample, and l is the length between the electrodes. Rectangular samples were dehydrated at 60 °C under vacuum until constant weight, and the weight (W_{dry}), thickness (T_{dry}), and length (L_{dry}) were tested. Then, the samples were immersed in water until fully hydrated, and the weight (W_{wet}), thickness (T_{wet}), and length (L_{wet}) were tested. The water uptake, through-plane swelling, and in-plane swelling were respectively calculated by the equations: water uptake (%) = $(W_{wet} - W_{dry})/W_{dry} \times 100$, ΔT (%) = $(T_{wet} - T_{dry})/T_{dry} \times 100$, and ΔL (%) = $(L_{wet} - L_{dry})/L_{dry} \times 100$. An electronic tensile machine (WDW-2, Yangzhou Zhongke Measuring Apparatus Co., China) was used to measure the mechanical properties of the dry membrane samples at a stretching rate of 1 mm min⁻¹ at room temperature. The weight-based ion exchange capacities (IEC_w) of the membranes were tested by acid-base titration method. The mechanical bendability of the GO/MMT/SPVA membranes was measured using an electronic tensile machine (WDW-2), in which the samples were subjected to repeated bending stress at a strain rate of 10 mm min⁻¹. The bendability was reflected by the number of bending cycles before a crack appeared in the sample.^[46] The resistance of the membranes to compression was measured using the following procedure. First, the membrane samples were compressed at a pressure of 1 MPa for 3 min, then the stress-strain curves were measured using an electronic tensile machine (WDW-2). The mechanical properties of compressed and noncompressed membranes were compared to evaluate the resistance to compression. A DMA

(Q800, TA Instrument) was used to measure the storage modulus of membrane. The chemical stability of membrane was evaluated by comparing the weight change of membranes after immersion in Fenton's reagent (3 wt% H₂O₂ containing 2 ppm FeSO₄) at 80 °C for 1 h, according to a standard accelerated oxidative stability test.^[32] The volume-based ion exchange capacities, IEC_v(dry) and IEC_v(wet) (mmol cm⁻³), are calculated, respectively, by the equations: IEC_v(dry) = IEC_w × ρ , and IEC_v(wet) = IEC_v(dry)/(1 + 0.01 WU × ρ), where ρ is the membrane density in the dry state. IEC_v(wet) can be regarded as the ion concentration in the membrane. The effective mobility (μ , cm² s⁻¹ V⁻¹) is calculated by the equation: $\mu = \sigma/[IEC_v(wet) \times F]$, where σ and F are the proton conductivity and the Faraday's constant, respectively.^[47] The MEA was made by sandwiching a GO/MMT/SPVA membrane or Nafion membrane between gas-diffusion electrodes by hot pressing method. The Pt/C catalyst (60 wt% Pt, Johnson Matthey) was used as the anodic and cathodic catalyst. The catalyst loading was 1 mg cm⁻² for both anode and cathode. The ionomer (Nafion) loading was 30 wt% for both cathode and anode. The MEA for GO/MMT/SPVA membrane was hot pressed at 50 °C with a pressure of 0.4 MPa for 3 min.^[48] The MEA for Nafion membrane was hot pressed at 135 °C with a pressure of 0.4 MPa for 3 min.

Supporting Information

Supporting Information is available from the Wiley Online Library or from the author.

Acknowledgements

The authors thank the financial support from the National Natural Science Foundation of China (No. 21490583), the National Science Fund for Distinguished Young Scholars (21125627), and the Program of Introducing Talents of Discipline to Universities (B06006). M.D.G. acknowledges funding from Tianjin University and the Chinese Government 1000 Plan for foreign experts.

Conflict of Interest

The authors declare no conflict of interest.

Keywords

2D channels, graphene composite, nacre structures, proton conduction, solid electrolyte membranes

Received: November 1, 2016

Revised: March 16, 2017

Published online: June 6, 2017

- [1] G. He, Z. Li, J. Zhao, S. Wang, H. Wu, M. D. Guiver, Z. Jiang, *Adv. Mater.* **2015**, *27*, 5280.
- [2] a) N. Li, M. D. Guiver, *Macromolecules* **2014**, *47*, 2175; b) C. H. Park, S. Y. Lee, D. S. Hwang, D. W. Shin, D. H. Cho, K. H. Lee, T. W. Kim, T. W. Kim, M. Lee, D. S. Kim, C. M. Doherty, A. W. Thornton, A. J. Hill, M. D. Guiver, Y. M. Lee, *Nature* **2016**, *532*, 480.
- [3] H. Zhang, P. K. Shen, *Chem. Rev.* **2012**, *112*, 2780.
- [4] S. Takamuku, P. Jannasch, *Adv. Energy Mater.* **2012**, *2*, 129.
- [5] N. Li, S. Y. Lee, Y.-L. Liu, Y. M. Lee, M. D. Guiver, *Energy Environ. Sci.* **2012**, *5*, 5346.

- [6] a) K.-H. Oh, M.-J. Choo, H. Lee, K. H. Park, J.-K. Park, J. W. Choi, *J. Mater. Chem. A* **2013**, *1*, 14484; b) H. Gao, B. Guo, J. Song, K. Park, J. B. Goodenough, *Adv. Energy Mater.* **2015**, *5*, 1402235; c) Y. Zhu, F. Wang, L. Liu, S. Xiao, Z. Chang, Y. Wu, *Energy Environ. Sci.* **2013**, *6*, 618.
- [7] a) H. W. Kim, H. W. Yoon, S. M. Yoon, B. M. Yoo, B. K. Ahn, Y. H. Cho, H. J. Shin, H. Yang, U. Paik, S. Kwon, J. Y. Choi, H. B. Park, *Science* **2013**, *342*, 91; b) R. R. Nair, H. A. Wu, P. N. Jayaram, I. V. Grigorieva, A. K. Geim, *Science* **2012**, *335*, 442.
- [8] R. K. Joshi, P. Carbone, F. C. Wang, V. G. Kravets, Y. Su, I. V. Grigorieva, H. A. Wu, A. K. Geim, R. R. Nair, *Science* **2014**, *343*, 752.
- [9] K. Hatakeyama, M. R. Karim, C. Ogata, H. Tateishi, A. Funatsu, T. Taniguchi, M. Koinuma, S. Hayami, Y. Matsumoto, *Angew. Chem., Int. Ed.* **2014**, *53*, 6997.
- [10] a) G. Titvinidze, K.-D. Kreuer, M. Schuster, C. C. de Araujo, J. P. Melchior, W. H. Meyer, *Adv. Funct. Mater.* **2012**, *22*, 4456; b) X.-F. Li, F. P. V. Paoloni, E. A. Weiber, Z.-H. Jiang, P. Jannasch, *Macromolecules* **2012**, *45*, 1447.
- [11] A. R. Koltonow, J. Huang, *Science* **2016**, *351*, 1395.
- [12] S. Wan, J. Peng, L. Jiang, Q. Cheng, *Adv. Mater.* **2016**, *28*, 7862.
- [13] L. J. Bonderer, A. R. Studart, L. J. Gauckler, *Science* **2008**, *319*, 1069.
- [14] P. Podsiadlo, A. K. Kaushik, E. M. Arruda, A. M. Waas, B. S. Shim, J. Xu, H. Nandivada, B. G. Pumplun, J. Lahann, A. Ramamoorthy, N. A. Kotov, *Science* **2007**, *318*, 80.
- [15] C.-P. Liu, C.-A. Dai, C.-Y. Chao, S.-J. Chang, *J. Power Sources* **2014**, *249*, 285.
- [16] W. S. Hummers, R. E. Offeman, *J. Am. Chem. Soc.* **1958**, *80*, 1339.
- [17] G. He, X. He, X. Wang, C. Chang, J. Zhao, Z. Li, H. Wu, Z. Jiang, *Chem. Commun.* **2016**, *52*, 2173.
- [18] J. Zhao, Y. Zhu, G. He, R. Xing, F. Pan, Z. Jiang, P. Zhang, X. Cao, B. Wang, *ACS Appl. Mater. Interfaces* **2016**, *8*, 2097.
- [19] A. Walther, I. Bjurhager, J. M. Malho, J. Pere, J. Ruokolainen, L. A. Berglund, O. Ikkala, *Nano Lett.* **2010**, *10*, 2742.
- [20] a) J. Wang, Q. Cheng, L. Lin, L. Jiang, *ACS Nano* **2014**, *8*, 2739; b) C. Teng, J. Qiao, J. Wang, L. Jiang, Y. Zhu, *ACS Nano* **2016**, *10*, 413.
- [21] P. Ming, Z. F. Song, S. S. Gong, Y. Y. Zhang, J. L. Duan, Q. Zhang, L. Jiang, Q. F. Cheng, *J. Mater. Chem. A* **2015**, *3*, 21194.
- [22] Y. Q. Li, T. Yu, T. Y. Yang, L. X. Zheng, K. Liao, *Adv. Mater.* **2012**, *24*, 3426.
- [23] H. Bai, F. Walsh, B. Gludovatz, B. Delattre, C. Huang, Y. Chen, A. P. Tomsia, R. O. Ritchie, *Adv. Mater.* **2016**, *28*, 50.
- [24] H. B. Yao, Z. H. Tan, H. Y. Fang, S. H. Yu, *Angew. Chem., Int. Ed.* **2010**, *49*, 10127.
- [25] A. Jackson, J. Vincent, R. Turner, *Proc. R. Soc. London, Ser. B* **1988**, *234*, 415.
- [26] X. Yu, A. Roy, S. Dunn, A. S. Badami, J. Yang, A. S. Good, J. E. McGrath, *J. Polym. Sci., Part A: Polym. Chem.* **2009**, *47*, 1038.
- [27] Z. Tang, N. A. Kotov, S. Magonov, B. Ozturk, *Nat. Mater.* **2003**, *2*, 413.
- [28] S. Gong, W. Cui, Q. Zhang, A. Cao, L. Jiang, Q. Cheng, *ACS Nano* **2015**, *9*, 11568.
- [29] E. Munch, M. E. Launey, D. H. Alsem, E. Saiz, A. P. Tomsia, R. O. Ritchie, *Science* **2008**, *322*, 1516.
- [30] H. B. Yao, J. Ge, L. B. Mao, Y. X. Yan, S. H. Yu, *Adv. Mater.* **2014**, *26*, 163.
- [31] Z. An, O. C. Compton, K. W. Putz, L. C. Brinson, S. T. Nguyen, *Adv. Mater.* **2011**, *23*, 3842.
- [32] S. Y. Lee, N. R. Kang, D. W. Shin, C. H. Lee, K.-S. Lee, M. D. Guiver, N. Li, Y. M. Lee, *Energy Environ. Sci.* **2012**, *5*, 9795.
- [33] a) N. Asano, M. Aoki, S. Suzuki, K. Miyatake, H. Uchida, M. Watanabe, *J. Am. Chem. Soc.* **2006**, *128*, 1762; b) J. Miyake, M. Sakai, M. Sakamoto, M. Watanabe, K. Miyatake, *J. Membr. Sci.* **2015**, *476*, 156; c) K. Yamazaki, Y. Tang, H. Kawakami, *J. Membr. Sci.* **2010**, *362*, 234; d) K. Miyatake, Y. Chikashige, E. Higuchi, M. Watanabe, *J. Am. Chem. Soc.* **2007**, *129*, 3879.
- [34] W. Liu, S. Wang, M. Xiao, D. Han, Y. Meng, *Chem. Commun.* **2012**, *48*, 3415.
- [35] G. He, J. Zhao, S. Hu, L. Li, Z. Li, Y. Li, Z. Li, H. Wu, X. Yang, Z. Jiang, *ACS Appl. Mater. Interfaces* **2014**, *6*, 15291.
- [36] C. Laberty-Robert, K. Valle, F. Pereira, C. Sanchez, *Chem. Soc. Rev.* **2011**, *40*, 961.
- [37] G. He, C. Chang, M. Xu, S. Hu, L. Li, J. Zhao, Z. Li, Z. Li, Y. Yin, M. Gang, H. Wu, X. Yang, M. D. Guiver, Z. Jiang, *Adv. Funct. Mater.* **2015**, *25*, 7502.
- [38] N. Li, C. Wang, S. Y. Lee, C. H. Park, Y. M. Lee, M. D. Guiver, *Angew. Chem., Int. Ed.* **2011**, *50*, 9158.
- [39] K. Nakabayashi, T. Higashihara, M. Ueda, *Macromolecules* **2010**, *43*, 5756.
- [40] T. J. Peckham, S. Holdcroft, *Adv. Mater.* **2010**, *22*, 4667.
- [41] J.-J. Shao, K. Raidongia, A. R. Koltonow, J. Huang, *Nat. Commun.* **2015**, *6*, 7602.
- [42] W. Gao, G. Wu, M. T. Janicke, D. A. Cullen, R. Mukundan, J. K. Baldwin, E. L. Brosha, C. Galande, P. M. Ajayan, K. L. More, A. M. Dattelbaum, P. Zelenay, *Angew. Chem., Int. Ed.* **2014**, *53*, 3588.
- [43] S. Moghaddam, E. Pengwang, Y.-B. Jiang, A. R. Garcia, D. J. Burnett, C. J. Brinker, R. I. Masel, M. A. Shannon, *Nat. Nanotechnol.* **2010**, *5*, 230.
- [44] K.-D. Kreuer, *Chem. Mater.* **2014**, *26*, 361.
- [45] Z. Li, Z. Jiang, H. Tian, S. Wang, B. Zhang, Y. Cao, G. He, Z. Li, H. Wu, *J. Power Sources* **2015**, *288*, 384.
- [46] H.-J. Ha, E.-H. Kil, Y. H. Kwon, J. Y. Kim, C. K. Lee, S.-Y. Lee, *Energy Environ. Sci.* **2012**, *5*, 6491.
- [47] Z. Li, W. Wang, Y. Chen, C. Xiong, G. He, Y. Cao, H. Wu, M. D. Guiver, Z. Jiang, *J. Mater. Chem. A* **2016**, *4*, 2340.
- [48] K. Scott, *Chem. Commun.* **2012**, *48*, 5584.